Advances in Applied Mathematics and Mechanics
Adv. Appl. Math. Mech., Vol. **3**, No. 3, pp. 280-296

DOI: 10.4208/aamm.10-10s2-02
June 2011

Radiative Effects on Mixed Convection in a Uniformly Heated Vertical Convergent Channel with an Unheated Moving Plate

Assunta Andreozzi*, Nicola Bianco and Vincenzo Naso

DETEC-Università di Napoli Federico II, P.le Tecchio, 80-80125, Napoli, Italy

Received 21 January 2010; Accepted (in revised version) 4 November 2010
Available online 28 February 2011

Abstract. Fluids engineering is extremely important in a wide variety of materials processing systems, such as soldering, welding, extrusion of plastics and other polymeric materials, Chemical Vapor Deposition (CVD), composite materials manufacturing. In particular, mixed convection due to moving surfaces is very important in these applications. Mixed convection in a channel, as a result of buoyancy and motion of one of its walls has received little research attention and few guidelines are available for choosing the best performing channel configuration, particularly when radiative effects are significant. In this study a numerical investigation of the effect of radiation on mixed convection in air due to the interaction between a buoyancy flow and an unheated moving plate induced flow in a uniformly heated convergent vertical channel is carried out. The moving plate has a constant velocity and moves in the buoyancy force direction. The principal walls of the channel are heated at uniform heat flux. The numerical analysis is accomplished by means of the commercial code Fluent. The effects of the wall emissivity, the minimum channel spacing, the converging angle and the moving plate velocity are investigated and results in terms of air velocity and temperature fields inside the channel and wall temperature profiles, both of the moving and the heated plates, are given. Nusselt numbers, both accounting and not for the radiative contribution to heat removal, are also presented.

AMS subject classifications: 80M12, 80A20
Key words: Mixed convection, moving surfaces, convergent channels, radiative effects.

1 Introduction

Mixed convection due to moving surfaces is very important in a wide variety of materials processing systems, such as soldering, welding, extrusion of plastics and other

*Corresponding author.
URL: `https://www.docenti.unina.it/assunta.andreozzi`
Email: assunta.andreozzi@unina.it (A. Andreozzi), nicola.bianco@unina.it (N. Bianco), vincenzo.naso@unina.it (V. Naso)

 ©2011 Global Science Press

polymeric materials, hot rolling, cooling and/or drying of paper and textiles, Chemical Vapor Deposition (CVD), composite materials manufacturing, as reviewed in [1–3]. Mixed convection with continuously moving vertical surfaces in a quiescent fluid was mostly investigated with reference to a single moving plate, as reported in [4, 5].

An analytical investigation on forced, mixed and natural convection for vertical and inclined moving sheets was carried out in [6]. The investigation underlined a significant velocity overshoot within the boundary layer as the buoyancy parameter increased and the buoyancy effect was more pronounced at lower Prandtl numbers. Correlations for inclined moving surfaces in mixed convection either with uniform surface heat flux or with uniform surface temperature were developed in [7]. The effect of buoyancy forces on flow and heat transfer over a moving heated vertical or inclined surface in a fluid was studied in [8]. The surface moved at non-uniform velocity and both the uniform wall temperature and uniform wall heat flux conditions were considered. The Nusselt number increased with the buoyancy parameter, the Prandtl number and the stream-wise distance. Moreover, the Nusselt number for the uniform wall heat flux case was larger than that in the uniform wall temperature case.

The effects of the radiation in the numerical and analytical analysis of heat transfer from a moving surface to the environment are very important. Kuiken [9] studied the heat transfer from a small continuously moving isothermal electric resistance to a still fluid. Karwe and Jaluria [10, 11] investigated numerically the heat transfer from a continuously moving isothermal plate to a still environment and compared predictions obtained by solving boundary layer equations with those obtained by solving complete elliptic equations.

Heat transfer in a convergent channel with two uniformly heated flat plates is also an interesting problem. The determination of the thermal performance of these configurations is rather difficult because of the large number of thermal and geometric variables, such as the converging angle, the minimum channel spacing and the imposed wall heat flux. Some papers dealt with natural convection in air in convergent channels [12–17]. A numerical study of steady, laminar, mixed convection heat transfer from volumetrically heat generating converging, parallel and diverging channels was carried out in [18]. Air was the working fluid. The maximum angle of deviation of the channel plates from the vertical position for the converging and diverging channels was 2° and -2°, respectively. A parametric study was carried out for a wide range of physical and geometrical parameters to investigate their effect on the fluid flow and heat transfer characteristics. A universal correlation was presented to evaluate the non-dimensional maximum temperature occurring in converging, parallel or diverging channels. A numerical investigation of mixed convection in air in a convergent vertical channel, due to the interaction between a buoyancy flow and a moving plate induced flow, was presented in [19]. The plate was adiabatic and moved at a constant velocity in the buoyancy force direction whereas the principal inclined walls of the channel were heated at uniform heat flux. The numerical analysis was carried out by means of the finite volume method, using the commercial code Fluent. The effects of the minimum channel spacing, wall heat flux, moving plate

velocity and converging angle were investigated. The effect of the converging angle on the wall temperatures was less marked at the larger channel spacing. Nusselt, Reynolds and Richardson numbers were correlated by a monomial equation for each converging angle and a unique monomial correlation for all investigated angles in the $2.1 \times 10^{-2} - 5.1 \times 10^{5}$ Richardson number range was presented. The same configuration was analyzed in [20]. The effects of the channel spacing, the wall heat flux, the moving plate velocity and the converging angle on the air streamlines and temperature fields were investigated. For all analyzed heat fluxes, streamlines showed that, when mere natural convection occurred, buoyancy forces drew upwards the air in the channel. Moreover, downstream of the channel exit section the air mass flow rate leaving the channel dragged some air mass flow rate from the surrounding ambient. When the adiabatic plate moved, air was dragged upwards not only by buoyancy forces but also by the moving plate. The temperature fields confirmed the fluid dynamic behavior in the analyzed system.

To the authors' knowledge, there are few studies on the radiation effects on mixed convection in a heated vertical convergent channel with a moving plate.

In the present study the numerical investigation presented in [19, 20] has been extended to the analysis of radiation effects. The principal walls of the channel are heated at uniform heat flux. In the mid-plane of the channel an unheated plate moves at a constant velocity in the buoyancy force direction. The problem is solved numerically and results are obtained by means of a finite volume method. Heat conduction in the heated plate together with radiative heat transfer is considered. The effects of the wall emissivity, the minimum channel spacing, the converging angle and the moving plate velocity are investigated and results in terms of air velocity and temperature fields inside the channel and wall temperature profiles, both of the moving and the heated plates, are given. Nusselt numbers, both accounting and not for the radiative contribution to heat removal, are also presented.

2 Mathematical description and numerical procedure

The investigated physical domain is shown in Fig. 1(a). It consists of a vertical convergent channel with an auxiliary unheated moving plate placed in its mid-plane. The moving plate, also termed "belt", moves at a constant velocity in the buoyancy force direction. Channel walls are heated at uniform heat flux, q_w, and are thermally conductive. The moving plate and the channel walls are assumed to be grey. The length of the heated plates is L, their thickness is s, the minimum channel spacing is b. The converging angle is θ. The working fluid is air.

The mixed convective flow in the vertical convergent channel is assumed to be incompressible. Moreover the system is assumed to be wide enough along the third coordinate to allow a 2D approximation. All thermophysical properties of the fluid are assumed to be constant, except for the dependence of density on the temperature (Boussinesq approximation). The thermophysical properties of the fluid are evalu-

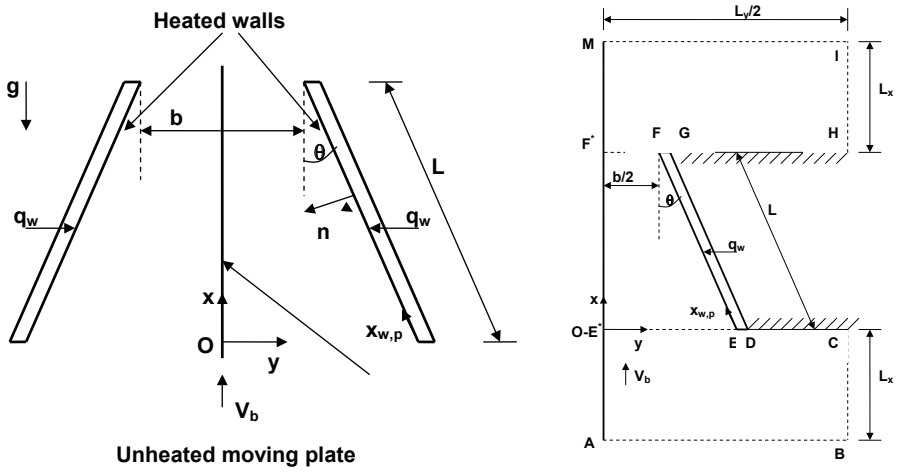

(a) (b)

Figure 1: Sketch of the system: (a) physical domain; (b) computational domain.

ated at the ambient temperature, T_0, which is assumed to be 300K in all cases. The surroundings are assumed to be a black body at the temperature of 300K.

The governing equations, for the fluid region in steady state regime, are time-averaged mass, Navier-Stokes and energy equations. A two-dimensional conduction model in the heated wall is employed whereas the transport equations for k and ε are formulated using the RNG $k-\varepsilon$ model. The radiative heat flux from the heated walls is then computed as the sum of the reflected fraction of the incident flux and the emitted flux

$$q_{out} = (1-\varepsilon_w)q_{in} + \varepsilon_w \sigma T_w^4, \tag{2.1}$$

where

$$q_{in} = \int_{r\cdot n>0} Ir \cdot n d\Omega, \tag{2.2}$$

with I the irradiation, W/m^2; r the direction of the irradiation; n the normal to the heated wall surface; Ω the solid angle, sr.

Nusselt numbers will be based on the difference between the heated walls and the inlet fluid temperatures, rather than on that between the heated walls and the bulk fluid temperatures, since the latter one cannot be easily measured in practical applications. The channel Nusselt number and the overall channel Nusselt number are defined as:

$$Nu = \frac{q_c b}{(\overline{T}_{w,p} - T_0)k_f}, \qquad Nu^* = \frac{(q_c + q_r)b}{(\overline{T}_{w,p} - T_0)k_f}, \tag{2.3}$$

where $\overline{T}_{w,p}$ is the average surface temperature of the heated plates

$$\overline{T}_{w,p} = \frac{1}{L}\int_0^L T_{w,p}(x_{w,p})dx_{w,p},$$

Table 1: Boundary conditions for the fluid domain.

u	v	T	Zone
$\frac{\partial u}{\partial y}=0$	$\frac{\partial v}{\partial y}=0$	$T_f=300K$ or $\frac{\partial T_f}{\partial y}=0$	BC, HI
$\frac{\partial u}{\partial x}=0$	$\frac{\partial v}{\partial x}=0$	$T_f=300K$ or $\frac{\partial T_f}{\partial x}=0$	AB, IM
$u=0$	$v=0$	$\pm k_f\frac{\partial T_f}{\partial x}+q_r=0$	CD, GH
$u=0$	$v=0$	$k_f\frac{\partial T_f}{\partial x}\pm q_r=k_s\frac{\partial T_s}{\partial x}$ and $T_s=T_f$	DE, FG
$u=0$	$v=0$	$k_f\frac{\partial T_f}{\partial n}=k_s\frac{\partial T_s}{\partial n}+q_w+q_r$ and $T_s=T_f$	EF
$u=V_b$	$v=0$	$-k_f\frac{\partial T_f}{\partial y}+q_r=0$	AM

Table 2: Boundary conditions for the solid domain.

T	Zone
$k_f\frac{\partial T_f}{\partial n}=k_s\frac{\partial T_s}{\partial n}+q_w+q_r$ and $T_s=T_f$	EF
$k_f\frac{\partial T_f}{\partial x}\pm q_r=k_s\frac{\partial T_s}{\partial x}$ and $T_s=T_f$	DE, FG
$\frac{\partial T_s}{\partial n}=0$	GD

and q_c and q_r are the spatially-averaged convective and radiative heat fluxes, respectively

$$q_c=\frac{1}{L}\int_0^L q_c(x_{w,p})dx_{w,p},\qquad q_r=\frac{1}{L}\int_0^L q_r(x_{w,p})dx_{w,p}. \tag{2.4}$$

It is worth noticing that a separate evaluation of q_c and q_r is very difficult in practice. The sum q_c+q_r is not equal to the dissipated heat flux q_w because of the conductive heat losses toward the ambient through the lower and upper edges of the walls.

From a numerical point of view an enlarged computational domain has been chosen. It is made up of the channel and of two L_x high and L_y wide reservoirs downstream and upstream of the channel, to simulate the free-stream conditions of the flow far away from the region of the thermal disturbance induced by the heated channel walls. The moving plate extends from the lower to the upper reservoir and its height is $L_b=L\cos\theta+2L_x$. Thanks to thermofluidynamic and geometrical symmetries, the problem is solved in half the domain, as shown in Fig. 1(b). The boundary conditions for the fluid and solid domains are reported in Tables 1 and 2, respectively, where q_w is the imposed wall heat flux introduced in the model as a flux discontinuity at the solid-fluid interface.

The commercial CFD code Fluent was employed to solve the governing equations. The SIMPLE scheme was chosen to couple pressure and velocity. The comparison between results obtained with Discrete Ordinates (DO) and Discrete Transfer Radiative Model (DTRM) in terms of heated plate and belt temperature profiles is reported in Fig. 2, for $q_w=120\text{W/m}^2$, $b=20\text{mm}$, $\theta=10^\circ$ and $V_b=1\text{m/s}$. The maximum percent difference between temperature values obtained with the two models was about 4%. The DO model was chosen [21]. The converging criteria were 10^{-6} for the residuals of the velocity components and 10^{-8} for the residuals of the energy.

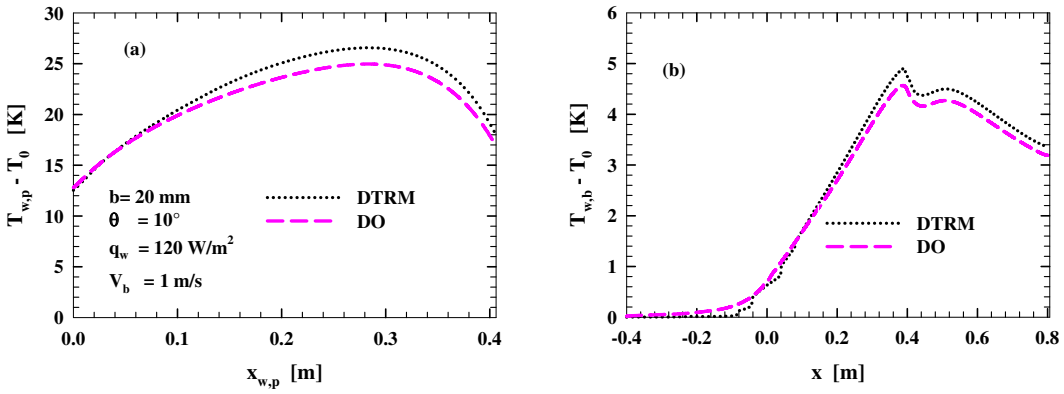

(a) (b)

Figure 2: Comparison between wall temperatures predicted by DTRM and DO radiative models, for $q_w = 120\text{W/m}^2$, $b = 20\text{mm}$, $\theta = 10^\circ$ and $V_b = 1\text{m/s}$: (a) heated plate; (b) unheated plate.

Preliminary results showed that the chosen turbulent model (RNG $k-\varepsilon$) was suitable also for laminar flow. Moreover, the RNG $k-\varepsilon$ was chosen because it provides an analytically-derived differential formula for effective viscosity that accounts for low Reynolds number effects. The enhanced wall treatment approach was employed since it is the most suitable when low-Reynolds-number affects the whole flow domain and for buoyancy-driven flows [21]. Several preliminary tests were carried out to make due allowance for the effect of turbulence parameters, k and ε, at the inlet. Assuming that the fluid comes from a quiescent zone, the distributions for k and ε were taken as uniform and equal to 10^{-6}. Moreover, the pressure upstream and downstream of the channel is set equal to the ambient pressure far away from the region of the thermal disturbance induced by the channel heated plate.

A preliminary study was performed to determine such a grid as to ensure its independence of the main variables, such as the channel Nusselt number. Computations have been made for $\theta = 10^\circ$, $b = 20\text{mm}$, $q_w = 30$ and 120W/m^2 and $V_b = 0$ and 1.0m/s on three different grids, as reported in Table 3. The maximum percent difference between the channel Nusselt number value predicted with mesh 2 and mesh 3 is 3.0% when the belt is motionless and 2.5% for $V_b = 1\text{m/s}$. Thus, results reported in this paper have been obtained with the mesh 2, which ensured a good compromise between the computational time and the accuracy. The $L_x = 0.400\text{m}$ and $L_y = 0.800\text{m}$ reservoirs dimensions ensure that solution to the problem is independent of the reservoirs size.

Table 3: Number of subdivisions of the computational domain for three different meshes.

Mesh	Convergent channel	Reservoirs
# 1	160×16	120×120
# 2	320×32	240×240
# 3	640×64	480×480

3 Results and discussion

In the following air streamlines and temperature fields are presented for air ($Pr = 0.71$), for a heated plates length $L = 0.406$m, for minimum channel spacings $b = 10$ and 20mm, for a wall heat flux $q_w = 120\text{W/m}^2$, for convergence angles $\theta = 0^\circ$, 2° and 10°, for belt velocities $V_b = 0$ and 1m/s. The heated plates thickness s is equal to 3.2mm. When $V_b = 0$m/s pure natural convection occurs. Predictions obtained using a model with negligible radiative heat transfer will be compared with predictions derived assuming the heated walls of the channel and the moving plate to be grey with surface emissivities equal to 0.90 and 0.20, respectively.

Air streamlines, for $q_w = 120\text{W/m}^2$, $b = 10$mm, $\theta = 2^\circ$ and for all the investigated values of the belt velocity and the walls emissivity are presented in Figs. 3(a) and (b), where radiative heat transfer is neglected, and in Figs. 3(c) and (d), where radiation is accounted for. Fig. 3(a) shows that when mere natural convection ($V_b = 0$m/s) occurs and radiation is not taken into account ($\varepsilon_p = \varepsilon_b = 0$) buoyancy forces draw the air upwards in the channel. The closer the fluid to the heated wall the stronger the buoyancy forces effects and, therefore, the larger the velocity of the fluid. Turning to the case with $V_b = 0$m/s and $\varepsilon_p = 0.90$ and $\varepsilon_b = 0.20$, Fig. 3(c) exhibits a distribution of the streamlines similar to that in Fig. 3(a), with the velocity of the fluid near the unheated plate larger than that with $\varepsilon_p = \varepsilon_b = 0$. The increase in the fluid velocity depends on the increase in the temperature of the unheated plate that, on turn, depends on the irradiative from the heated walls of the channel. When the belt moves air is dragged upwards both with (Fig. 3(d)) and without (Fig. 3(b)) radiative heat transfer and we can notice that the fluid velocity is larger in the proximity of the moving plate. The similar distribution of the streamlines in the two afore mentioned cases indicates that the fluid velocity is mainly affected by drag forces. One can argue that when the belt moves, the fluid flow is nearly independent of the buoyancy forces.

In order to appreciate the effect of the boundary conditions used in this work, a picture reporting air streamlines in the whole computational domain is presented in Fig. 4 for $q_w = 120\text{W/m}^2$, $b = 10$mm, $\theta = 2^\circ$, $V_b = 1$m/s, $\varepsilon_p = 0.90$, $\varepsilon_b = 0.20$.

Air streamlines for $\theta = 10^\circ$, all other quantities being the same as those in Fig. 3, are presented in Fig. 5. As it was to be expected the comparison between each couple of corresponding configurations in Figs. 3 and 5 shows a larger effect of the radiation in those with the larger converging angle, because of the larger view factor between the channel walls and the surroundings. In Fig. 5(a), concerning natural convection with no radiation, a counter-clockwise vortex in the channel can be noticed. As a matter of fact, because of the marked decrease in the cross sections of the converging channel, not all the air flow rate dragged upwards from the lower reservoir by buoyancy forces exits the end section of the channel. Consequently, the air flow chokes and a vortex region occurs in the channel. The effect of radiation is pointed out in Fig. 5(c), where air velocities larger than those in Fig. 5(a) are exhibited close to the unheated still plate, whose temperature is increased by radiation from the heated walls. A fraction of the air flow rate is first dragged downwards in the channel and then buoyancy forces close

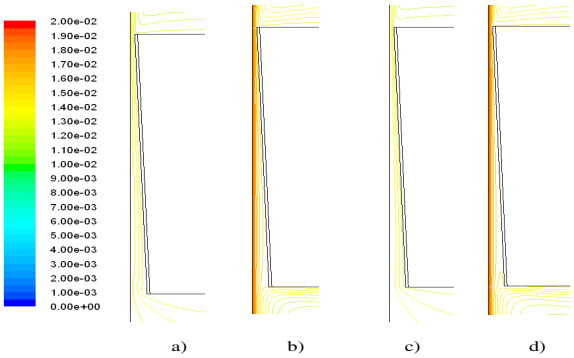

Figure 3: Air streamlines (kg/sm^2), for $q_w = 120\text{W/m}^2$, $b = 10\text{mm}$ and $\theta = 2°$: (a) $V_b = 0\text{m/s}$, $\varepsilon_p = \varepsilon_b = 0$; (b) $V_b = 1\text{m/s}$, $\varepsilon_p = \varepsilon_b = 0$; (c) $V_b = 0\text{m/s}$, $\varepsilon_p = 0.90$, $\varepsilon_b = 0.20$; (d) $V_b = 1\text{m/s}$, $\varepsilon_p = 0.90$, $\varepsilon_b = 0.20$.

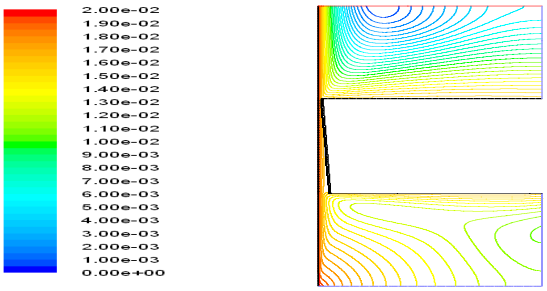

Figure 4: Air streamlines (kg/sm^2), for $q_w = 120\text{W/m}^2$, $b = 10\text{mm}$, $\theta = 2°$; $V_b = 1\text{m/s}$, $\varepsilon_p = 0.90$, $\varepsilon_b = 0.20$.

to the heated wall drag it upward. Similar considerations can be made as far as the mixed convection configurations are concerned (Figs. 5(b) and (d)). The moving plate drags air from the lower reservoir but the flow rate is too large to allow the whole air mass flow rate to reach the exit section of the convergent channel and, therefore, a fraction of the flow inverts its direction and moves back to the inlet section of the

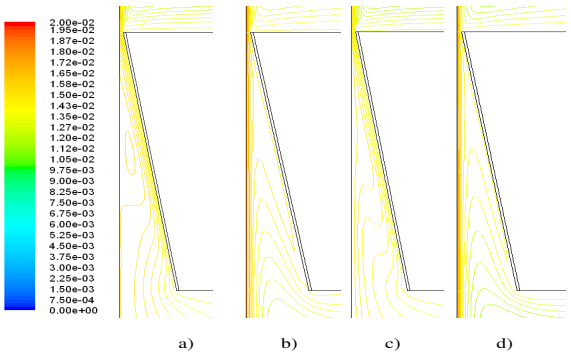

Figure 5: Air streamlines (kg/sm^2), for $q_w = 120\text{W/m}^2$, $b = 10\text{mm}$ and $\theta = 10°$: (a) $V_b = 0\text{m/s}$, $\varepsilon_p = \varepsilon_b = 0$; (b) $V_b = 1\text{m/s}$, $\varepsilon_p = \varepsilon_b = 0$; (c) $V_b = 0\text{m/s}$, $\varepsilon_p = 0.90$, $\varepsilon_b = 0.20$; (d) $V_b = 1\text{m/s}$, $\varepsilon_p = 0.90$, $\varepsilon_b = 0.20$.

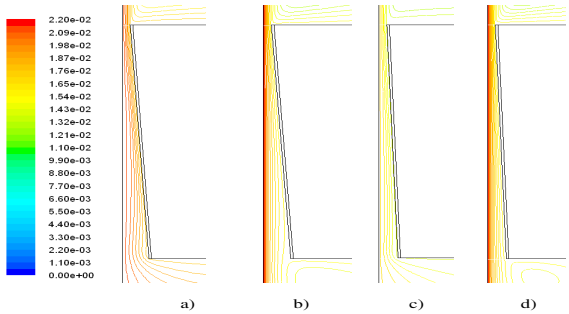

Figure 6: Air streamlines (kg/sm^2), for $q_w = 120\text{W/m}^2$, $b = 20\text{mm}$ and $\theta = 2°$: (a) $V_b = 0\text{m/s}$, $\varepsilon_p = \varepsilon_b = 0$; (b) $V_b = 1\text{m/s}$, $\varepsilon_p = \varepsilon_b = 0$; (c) $V_b = 0\text{m/s}$, $\varepsilon_p = 0.90$, $\varepsilon_b = 0.20$; (d) $V_b = 1\text{m/s}$, $\varepsilon_p = 0.90$, $\varepsilon_b = 0.20$.

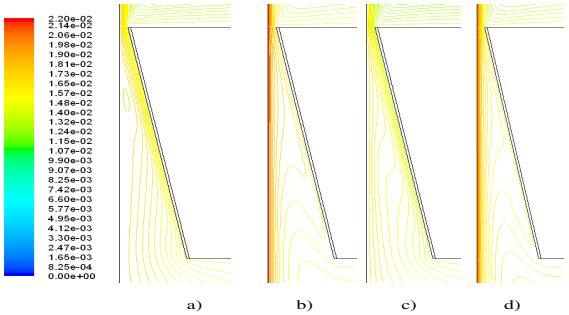

Figure 7: Air streamlines (kg/sm^2), for $q_w = 120\text{W/m}^2$, $b = 20\text{mm}$ and $\theta = 10°$: (a) $V_b = 0\text{m/s}$, $\varepsilon_p = \varepsilon_b = 0$; (b) $V_b = 1\text{m/s}$, $\varepsilon_p = \varepsilon_b = 0$; (c) $V_b = 0\text{m/s}$, $\varepsilon_p = 0.90$, $\varepsilon_b = 0.20$; (d) $V_b = 1\text{m/s}$, $\varepsilon_p = 0.90$, $\varepsilon_b = 0.20$.

channel. A part of it is, on turn, dragged upwards by buoyancy forces close to the heated wall. This effect is less marked in Fig. 5(d) than in Fig. 5(b), since the effect of buoyancy forces is smaller when radiation contributes to the heat transfer.

Air streamlines for $b = 20\text{mm}$, all other quantities being the same as those in Fig. 3, are presented in Fig. 6. Fig. 6(a), like Fig. 3(a), shows that velocities of the air are larger in the proximity of the heated walls whereas one can remark that radiation increases

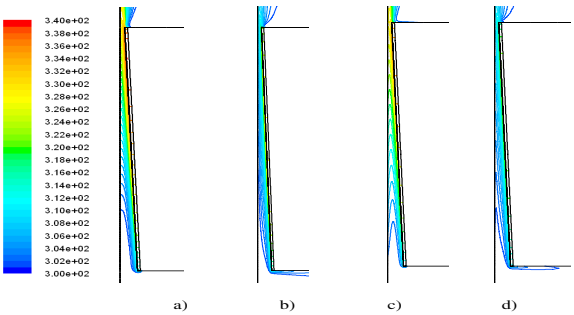

Figure 8: Air temperature (K), for $q_w = 120\text{W/m}^2$, $b = 10\text{mm}$ and $\theta = 2°$: (a) $V_b = 0\text{m/s}$, $\varepsilon_p = \varepsilon_b = 0$; (b) $V_b = 1\text{m/s}$, $\varepsilon_p = \varepsilon_b = 0$; (c) $V_b = 0\text{m/s}$, $\varepsilon_p = 0.90$, $\varepsilon_b = 0.20$; (d) $V_b = 1\text{m/s}$, $\varepsilon_p = 0.90$, $\varepsilon_b = 0.20$.

the air velocity near the motionless belt. Figs. 6(b) and (d) show that the upward moving belt allows the whole air flow rate to exit the end section of the channel.

Air streamlines for $\theta = 10^\circ$, all other quantities being the same as those in Fig. 6, are presented in Fig. 7. We can remark in Fig. 7(a) a recirculation region in the channel, whose extension, thanks to the larger exit section of the channel, is, however, smaller than that exhibited in Fig. 5(a), where reference was made to the same configuration apart from the difference in the minimum spacing ($b = 10$mm instead of $b = 20$mm). Similarly to what occurred in the case for $b = 10$mm, also in the present case there is no vortex when the radiative contribution is taken into account (Fig. 7(c)). Although in the mixed convection configuration the distribution of streamlines in Figs. 7(b) and 5b as well as in Figs. 7(d) and 5(d) is very similar, we can notice that when $b = 20$mm a larger fraction of the air flow rate reaches the exit section of the channel, because of the larger spacing.

Air temperature fields for the same value of the process parameters as those in Figs. 3, 5, 6, 7 are presented in Figs. 8-11, respectively. As far as the limiting case of natural convection and no contribution of radiation is concerned, Fig. 8(a) points out a developing thermal field in the lower half region near the heated wall of the channel, whereas a thin thermal boundary layer on the motionless belt is also exhibited in Fig. 8(c), since in this case the contribution of the radiative heat transfer from the heated walls raises the temperature of the belt. The maximum temperature of the air is nearly the same in both cases. Passing from natural (Figs. 8(a) and (c)) to mixed convection (Figs. 8(b) and (d)), we can notice that, both with and without the radiative contribution, in the latter configuration the thermal boundary layer along the heated wall is thinner and the air temperature is lower. Figs. 8(b) and (d) point out that the difference between the maximum air temperatures determined by the radiative contribution is always no larger than about 5K.

The comparison of Fig. 9 to Fig. 8 shows that increasing the converging angle determines a slight increase in air temperatures. This is likely due to the recirculation regions pointed out in Fig. 5, that choke the air flow, thus increasing air temperature. Fig. 9(a) shows that the thermal field starts to develop near the leading edge of the heated wall. The development of the temperature field ends in the region of the channel where the counter-clockwise vortex shown in Fig. 5(a) is located. One can also notice that air close to the motionless belt starts to warm up in the channel region where the vortex adjacent to the belt is transferring warmer air. In Fig. 9(c) slightly lower temperatures and a developing temperature field also along the belt heated by radiation from the channel wall are exhibited. The comparison of Figs. 9(b) and (d) to the corresponding Figs. 9(a) and (c) points out both a larger dependence of temperatures on radiation and a far lower temperature of the belt in mixed than in natural convection. Therefore one can conclude that the contribution of radiation to the heat removal is larger when the belt moves.

Comparing Fig. 10 to Fig. 8 and Fig. 9 to Fig. 11, one can notice that increasing the minimum channel spacing decreases the air temperature. Figs. 10(a) and (c) as well as Figs. 10(b) and (d) allow to conclude that both in natural convection and in

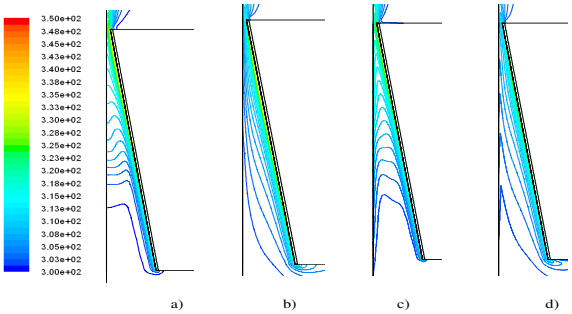

Figure 9: Air temperature (K), for $q_w = 120\text{W/m}^2$, $b = 10\text{mm}$ and $\theta = 10^\circ$: (a) $V_b = 0\text{m/s}$, $\varepsilon_p = \varepsilon_b = 0$; (b) $V_b = 1\text{m/s}$, $\varepsilon_p = \varepsilon_b = 0$; (c) $V_b = 0\text{m/s}$, $\varepsilon_p = 0.90$, $\varepsilon_b = 0.20$; (d) $V_b = 1\text{m/s}$, $\varepsilon_p = 0.90$, $\varepsilon_b = 0.20$.

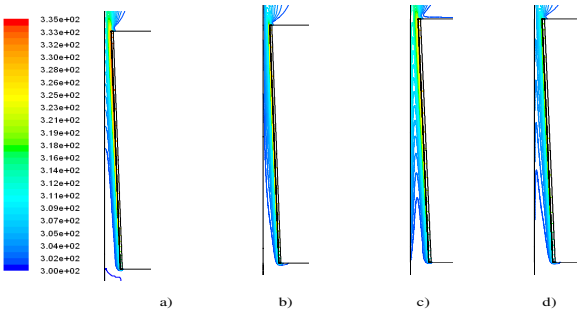

Figure 10: Air temperature (K), for $q_w = 120\text{W/m}^2$, $b = 20\text{mm}$ and $\theta = 2^\circ$: (a) $V_b = 0\text{m/s}$, $\varepsilon_p = \varepsilon_b = 0$; (b) $V_b = 1\text{m/s}$, $\varepsilon_p = \varepsilon_b = 0$; (c) $V_b = 0\text{m/s}$, $\varepsilon_p = 0.90$, $\varepsilon_b = 0.20$; (d) $V_b = 1\text{m/s}$, $\varepsilon_p = 0.90$, $\varepsilon_b = 0.20$.

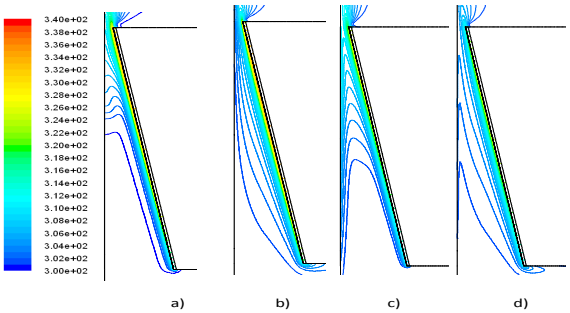

Figure 11: Air temperature (K), for $q_w = 120\text{W/m}^2$, $b = 20\text{mm}$ and $\theta = 10^\circ$: (a) $V_b = 0\text{m/s}$, $\varepsilon_p = \varepsilon_b = 0$; (b) $V_b = 1\text{m/s}$, $\varepsilon_p = \varepsilon_b = 0$; (c) $V_b = 0\text{m/s}$, $\varepsilon_p = 0.90$, $\varepsilon_b = 0.20$; (d) $V_b = 1\text{m/s}$, $\varepsilon_p = 0.90$, $\varepsilon_b = 0.20$.

mixed convection maximum air temperature in the configuration without radiation is slightly larger than that in configuration with radiation. Once again an increase in temperatures increasing the converging angle is exhibited in Fig. 11. Comparing Figs. 11(a) and (b) to Figs. 11(c) and (d) shows that in this configuration maximum temperatures with the radiative contribution are lower than without it.

Heated wall temperature profiles for $\theta = 0^\circ, 2^\circ, 10^\circ$, $b = 20\text{mm}$, $q_w = 120\text{W/m}^2$ and $V_b = 1\text{m/s}$ are reported in Fig. 12(a), for the cases where radiative heat transfer is taken into account, and in Fig. 12(b), for the cases where radiative heat transfer is neglected. The comparison between the two cases shows that temperature profiles for

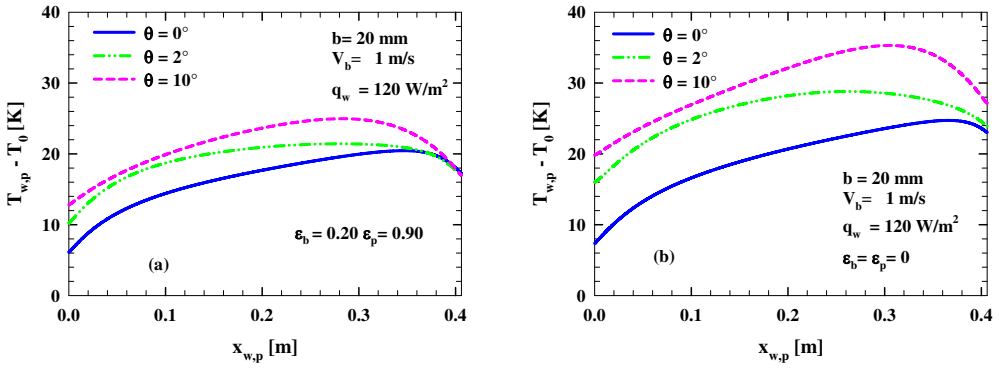

(a) (b)

Figure 12: Heated wall temperature profiles, for $q_w = 120\text{W/m}^2$, $b = 20\text{mm}$ and $V_b = 1\text{m/s}$: (a) $\varepsilon_p = 0.90$, $\varepsilon_b = 0.20$; (b) $\varepsilon_p = \varepsilon_b = 0$.

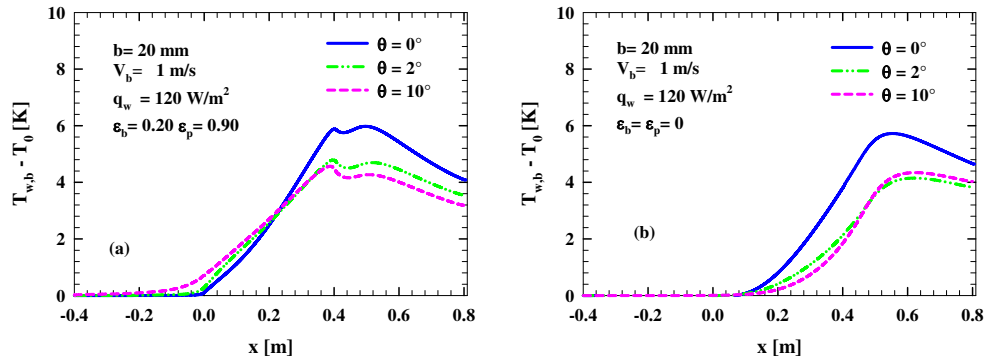

(a) (b)

Figure 13: Belt temperature profiles, for $q_w = 120\text{W/m}^2$, $b = 20\text{mm}$ and $V_b = 1\text{m/s}$: (a) $\varepsilon_p = 0.90$, $\varepsilon_b = 0.20$; (b) $\varepsilon_p = \varepsilon_b = 0$.

$\theta = 0°$ are nearly the same, except in the upper part of the walls, whereas temperatures are larger when radiative heat transfer is not accounted for, because of the larger values of both walls temperature and view factor toward the surroundings in this region of the channel. Differences between temperature profiles in the two compared cases increase as the converging angle increases, due to the increasing view factor toward the lower reservoir.

The comparison with the case with negligible radiative heat transfer, in terms of belt surface temperature profiles, is reported in Fig. 13 for the same values of process parameters as those in the previous figure. For the parallel walled channel ($\theta = 0°$), belt temperatures in the heated channel ($0 \leq x \leq 406\text{mm}$) are slightly larger in the case with thermal radiation ($\varepsilon_p = 0.90$ and $\varepsilon_b = 0.20$) than in the other case ($\varepsilon_p = \varepsilon_b = 0$), when the radiative heat transfer from the heated plate to the moving belt does not contribute to the heating of the moving plate. Outside of the heated channel, belt temperatures in the case with thermal radiation are smaller than those in the other

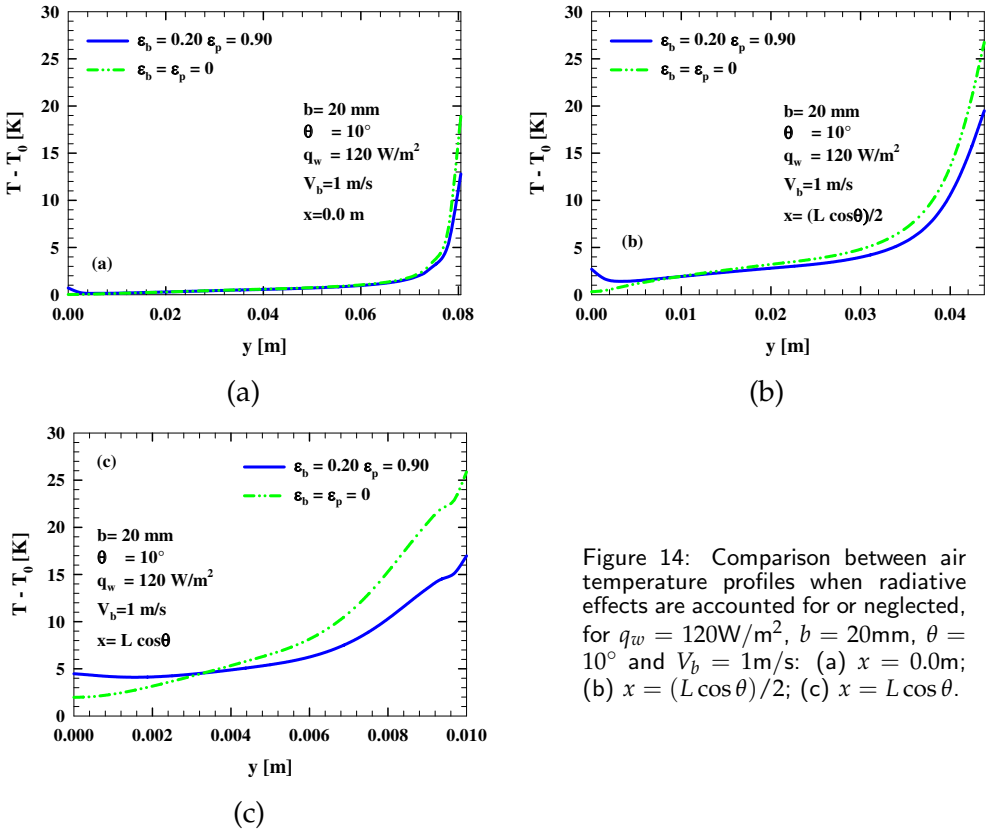

Figure 14: Comparison between air temperature profiles when radiative effects are accounted for or neglected, for $q_w = 120\text{W/m}^2$, $b = 20\text{mm}$, $\theta = 10^\circ$ and $V_b = 1\text{m/s}$: (a) $x = 0.0\text{m}$; (b) $x = (L\cos\theta)/2$; (c) $x = L\cos\theta$.

case, because of the larger cooling rate, caused by the radiative heat losses toward the surrounding. One can notice that in the case without thermal radiation the moving belt temperature begins to increase at an x value nearly equal to 0.12m, where the thermal boundary layer thickness becomes equal to the channel spacing and the hot fluid warms up the moving plate. When radiative heat transfer is taken into account, moving belt temperatures begin to increase at the heated channel inlet section, because of the radiative heat transfer and the view factor between the heated plate and the belt. Increasing the converging angle the abscissa at which the moving belt temperature begins to increase shifts upstream when radiative heat transfer is taken into account (Fig. 13(a)) whereas it shifts downstream when radiation is neglected (Fig. 13(b)).

Differences in the predictions when radiation effects are accounted for or neglected are pointed out in Figs. 14 and 15, where the profiles of air temperature and air x-component velocity along the y coordinate, respectively, in three sections of the channel, for $q_w = 120\text{W/m}^2$, $b = 20\text{mm}$, $\theta = 10^\circ$ and $V_b = 1\text{m/s}$: (a) $x = 0.0\text{m}$; (b) $x = (L\cos\theta)/2$; (c) $x = L\cos\theta$ are presented.

Fig. 14 shows that the larger the distance from the inlet section of the channel the larger the effect of the radiative contribution on the air temperature. One can also remark that in the exit section ($x = L\cos\theta$) the radiative contribution to the heat removal strongly lowers the air temperature close to the heated walls whereas the

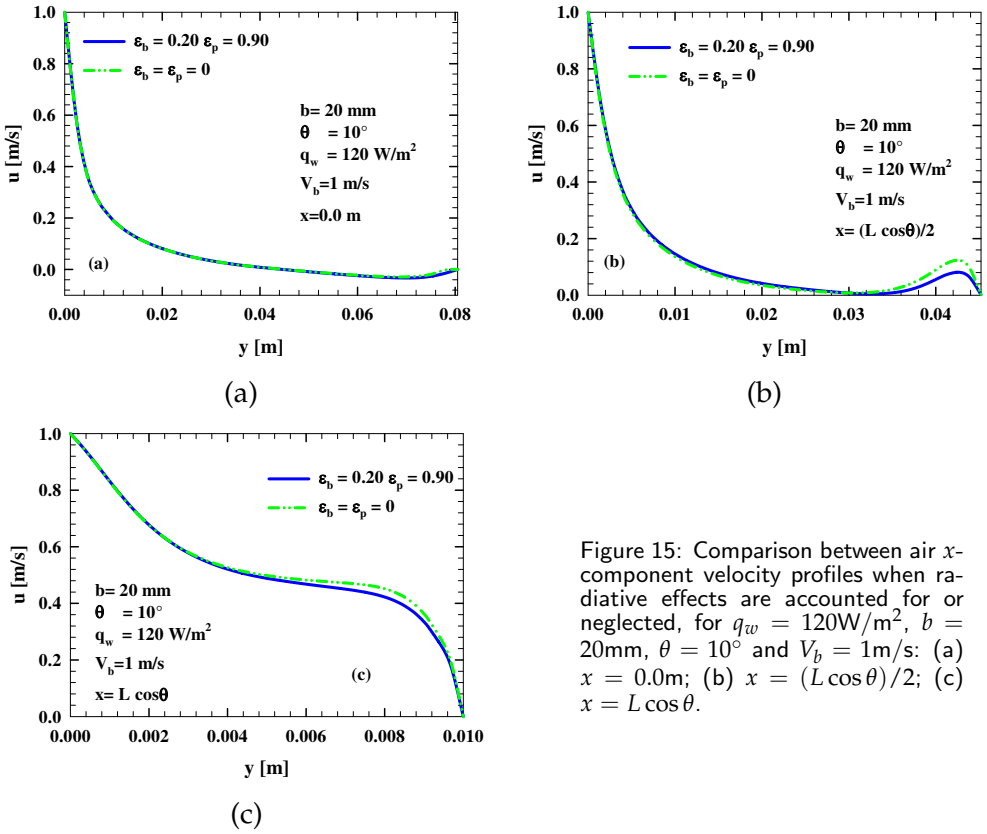

Figure 15: Comparison between air x-component velocity profiles when radiative effects are accounted for or neglected, for $q_w = 120\text{W/m}^2$, $b = 20\text{mm}$, $\theta = 10^\circ$ and $V_b = 1\text{m/s}$: (a) $x = 0.0\text{m}$; (b) $x = (L\cos\theta)/2$; (c) $x = L\cos\theta$.

opposite occurs in the proximity of the unheated belt.

In Fig. 15 one can remark that the x-component of the air velocity is nearly unaffected by the radiative contribution. However we can notice in the mid-height section of the channel (Fig. 15(b)) that larger surface temperatures of the heated walls increase air temperatures close to the surface that, on turn, increase the velocity of the air.

The channel Nusselt number and the overall channel Nusselt number, for $b = 10\text{mm}$ and 20mm, $V_b = 0$ and 1.0m/s, $\theta = 2^\circ$ and 10°, are presented in Tables 4 and 5, respectively.

Table 4: Channel Nusselt numbers.

	$b = 10\text{mm}$		$b = 20\text{mm}$	
	$V_b = 0\text{m/s}$	$V_b = 1\text{m/s}$	$V_b = 0\text{m/s}$	$V_b = 1\text{m/s}$
$\theta = 2^\circ$	1.39	1.94	3.16	3.79
$\theta = 10^\circ$	1.46	1.38	3.02	2.86

Table 5: Overall channel Nusselt numbers.

	$b = 10\text{mm}$		$b = 20\text{mm}$	
	$V_b = 0\text{m/s}$	$V_b = 1\text{m/s}$	$V_b = 0\text{m/s}$	$V_b = 1\text{m/s}$
$\theta = 2^\circ$	1.76	2.46	4.15	4.97
$\theta = 10^\circ$	2.06	2.12	4.41	4.48

4 Conclusions

The effect of radiation on mixed convection in air due to the interaction between a buoyancy flow and an unheated belt induced flow in a convergent vertical channel was investigated numerically. The belt was located in the channel mid-plane and moved at a constant velocity in the direction assisting the buoyancy effects, and the channel walls were heated at uniform heat flux. Results showed that the effects of thermal radiation were more marked when the belt was motionless. For the configuration with $\theta = 10^\circ$ and no radiation, a counter-clockwise vortex in the channel was noticed, that, on the contrary, was not detected when radiative heat transfer was taken into account. Temperature fields pointed out that the contribution of radiation to the heat removal was larger when mixed convection occurred. Maximum temperatures with radiative contribution were lower than without it. Wall temperature profiles showed that the abscissa at which the temperature of the moving belt began to increase, decreased at increasing converging angles when radiative heat transfer was taken into account, whereas the opposite occurred when radiation was neglected. The larger the distance from the inlet section of the channel the larger the effect of the radiative contribution on the air temperature. The x-component of the air velocity is nearly unaffected by the radiative contribution.

Nomenclature

b	minimum channel spacing, m
g	acceleration due to the gravity, m/s^2
I	irradiation, W/m^2
k	thermal conductivity, W/m K
L	heated plates length, m
L_b	unheated plate length, m
L_x	reservoirs height, m
L_y	reservoirs width, m
n	normal to the surface
Nu	channel Nusselt number
$Nu*$	overall channel Nusselt number
Pr	Prandtl number
q	heat flux, W/m^2
r	direction of the irradiation
s	heated plates thickness, m
T	temperature, K
u	velocity component along x, m/s
v	velocity component along y, m/s
V_b	unheated plate velocity, m/s
x, y	Cartesian coordinates, m

Greek symbols

ε	emissivity
θ	converging angle, degrees
σ	Stephan-Boltzmann constant, $W/m^2\ K^4$
Ω	solid angle, sr

Subscripts

b	moving plate (belt)
c	convective
f	fluid
in	incident
0	ambient
out	from the surface
p	heated plate
r	radiative
s	solid
w	wall

References

[1] R. VISKANTA AND T. L. BERGMAN, Heat Transfer in Materials Processing, in: W. M. Rohsenow, J. P. Hartnett, Y. I. Cho (Eds.), Handbook of Heat Transfer, McGraw-Hill, New York, 1998.

[2] Y. JALURIA, *Fluid flow phenomena in material processing*, J. Fluid. Eng., 123 (2001), pp. 173–210.

[3] Y. JALURIA, *Thermal processing of materials: from basic research to engineering*, J. Heat. Trans., 125 (2003), pp. 957–979.

[4] S. A. AL-SANEA, *Convection regimes and heat transfer characteristic along a continuous moving heated vertical plate*, Int. J. Heat. Fluid. Flow, 24 (2003), pp. 888–991.

[5] S. A. AL-SANEA, *Mixed convection heat transfer along a continuously moving heated vertical plate with suction or injection*, Int. J. Heat. Mass. Trans., 47 (2004), pp. 1445–1465.

[6] N. RAMACHANDRAN, T. S. CHEN AND B. F. ARMALY, *Mixed convection from vertical and inclined moving sheets in a parallel free stream*, J. Thermophys., 1(3) (1987), pp. 274–281.

[7] N. RAMACHANDRAN, T. S. CHEN AND B. F. ARMALY, *Correlations for laminar mixed convection in boundary layers adjacent to inclined, continuous, moving sheets*, Int. J. Heat. Mass. Trans., 30(10) (1987), pp. 2196–2199.

[8] A. J. CHAMKHA, H. S. TAKHAR AND G. NATH, *Effect of buoyancy force on the flow and heat transfer over a continuous moving vertical or inclined surface*, Int. J. Thermal. Sci., 40 (2001), pp. 825–833.

[9] H. K. KUIKEN, *The cooling of a low-heat-resistance cylinder moving through a fluid*, Proc. Soc. London., A346 (1975), pp. 23–35.

[10] M. V. KARWE AND Y. JALURIA, *Fluid flow and mixed convection transport from a plate in rolling and extrusion processes*, ASME J. Heat. Trans., 110 (1988), pp. 655–661.

[11] M. V. KARWE AND Y. JALURIA, *Numerical simulation of thermal transport associated with a continuously moving flat sheet in materials processing*, ASME J. Heat. Trans., 113 (1991), pp. 612–619.
[12] N. BIANCO AND S. NARDINI, *Numerical analysis of natural convection in air in a vertical convergent channel with uniformly heated conductive walls*, Int. Commun. Heat. Mass. Trans., 32 (2004), pp. 758–769.
[13] N. BIANCO, L. LANGELLOTTO, O. MANCA AND S. NARDINI, *Numerical analysis of radiative effects on natural convection in vertical convergent and symmetrically heated channels*, Numer. Heat. Trans., 49 (2006), pp. 369–391.
[14] K. D. KIHM, J. H. KIM AND L. FLETCHER, *Investigation of natural convection heat transfer in vertical converging channel flows using a specklegram technique*, J. Heat. Trans., 115 (1993), pp. 140–148.
[15] S. A. SAID, *Investigation of natural convection in convergent vertical channels*, Int. J. Energy. Res., 20 (1996), pp. 559–567.
[16] J. S. SHALASH, J. D. TARASUK AND D. NAYLOR, *Experimental and numerical studies of natural convection heat transfer in vertical converging channel flows*, Proc. 4th Int. Con. Experimental. Heat. Trans. Fluid. Mech. Thermodyn., 4 (1997), pp. 2167–2174.
[17] E. M. SPARROW, R. RUIZ AND L. F. A. AZEVEDO, *Experiments and numerical investigation of natural convection in convergent vertical channels*, Int. J. Heat. Mass. Trans., 31 (1988), pp. 907–915.
[18] B. PREMACHANDRAN AND C. BALAJI, *A correlation for mixed convection heat transfer from converging, parallel and diverging channels with uniform volumetric heat generating plates*, Int. Commun. Heat. Mass. Trans., 33 (2006), pp. 350–356.
[19] A. ANDREOZZI, N. BIANCO, G. LACASA AND V. NASO, *Mixed convection heat transfer in a convergent vertical channel with a moving plate*, Proc. 8th Biennial ASME Conference on Engineering Systems Design and Analysis (ESDA), paper no. ESDA2006-95502, Torino, July 4–7, 2006.
[20] A. ANDREOZZI, G. LACASA AND E. ROSSI DI SCHIO, *Numerical analysis of mixed convection in air in a convergent vertical channel with a moving plate*, JP J. Heat. Mass. Trans., 1(2) (2007), pp. 187–217.
[21] Fluent Inc., Fluent 6.2, User Manual, Lebanon, NH, 2005.